# Evaluation of treatment response of cilengitide in an experimental model of breast cancer bone metastasis using dynamic PET with $^{18}$F-FDG

**Caixia Cheng[1] PhD,**
**Dorde Komljenovic[2] PhD,**
**Leyun Pan[1] PhD,**
**Antonia Dimitrakopoulou-Strauss[1] MD,**
**Ludwig G. Strauss[1] MD,**
**Tobias Bäuerle[2] MD**

*1. Clinical Cooperation Unit Nuclear Medicine and*
*2. Department of Medical Physics in Radiology,*
*German Cancer Research Center, Heidelberg, Germany*

***

Keywords: PET – $^{18}$F-FDG
- Cilengitide
- MDA-MB-231 breast cancer cells
- Bone metastases

***Correspondence address:***
Caixia Cheng, PhD
Clinical Cooperation Unit Nuclear Medicine, German Cancer Research Center,
Im Neuenheimer Feld 280,
D-69120 Heidelberg, Germany
Email: c.cheng@dkfz.de

*Received:*
17 February 2011
*Accepted revised:*
1 March 2011

## Abstract

*The purpose* of this study was the assessment of the feasibility of dynamic positron emission tomography (PET) studies with fluorine-18 fluorodeoxyglucose ($^{18}$F-FDG) to quantify effects of the cyclic Arg-Gly-Asp peptide cilengitide, which targets the αvβ3 and αvβ5 integrin receptors in rats with breast cancer bone metastases. *Rats were inoculated* with MDA-MB-231 breast cancer cells, followed by the development of lytic lesions in the hind leg. Rats with lytic lesions were treated with cilengitide five times weekly on a continuous basis from days 30 to 55 after tumor cell inoculation. Dynamic PET studies with $^{18}$F-FDG were performed in untreated (n=9), controlled (n=4) and treated rats (n=6). The data were assessed using learning-machine two-tissue compartmental analysis. The *$^{18}$F-FDG kinetic parameters* obtained by two-tissue compartmental model learning-machine showed significant differences when individual parameters were compared between the control group and treated animals. Quantitative assessment of the tracer kinetics and the application of classification analysis to the data provided us with evidence to identify those tumors that demonstrated effect of cilengitide treatment. The transport rate K1 and the phosphorylation rate k3 were significantly different ($P$=0.033 and 0.038, respectively). Classification analysis based on support vector machines ranking feature elimination of the combination of PET parameters revealed an overall accuracy of 80.0% between treated animals and the control group. We were able to identify 83.3% treated animals compared with the control group based on k2 and VB. *In conclusion,* the results revealed that cilengitide treatment of experimental breast cancer bone metastases had a significant therapeutics impact on $^{18}$F-FDG kinetics.

*Hell J Nucl Med 2011; 14(1): 15-20* *Published on line: 26 March 2011*

## Introduction

Worldwide, breast cancer is the second most common type of cancer after lung cancer (10.4% of all cancer incidence, both sexes counted) and the fifth most common cause of cancer death [1]. Several treatment protocols including surgery, hormone treatment and chemotherapy as well as radiation treatment are already in use. Recently, antiangiogenic and antitumor effects of several drugs have been studied in experimental models and in patients with breast cancer [2-5]. These drugs significantly inhibited breast cancer progression and metastasis including metastases to bone [6].

The αvβ3 and αvβ5 integrins are cell adhesion molecules that play a vital role in tumor angiogenesis and metastatic spread [7, 8]. Especially, αvβ3 integrin promotes spontaneous metastasis of breast cancer to bone [9, 10]. Cilengitide (EMD 121974) is a cyclic arginine-glycine-aspartic acid containing peptide that binds to αvβ3 and αvβ5 with nanomolar affinity. In cell adhesion assays, it inhibited both αvβ3 and αvβ5 mediated cell adhesion with $IC_{50}$ values in the low micromolar range and inhibited angiogenesis in the chick chorioallantoic membrane and rabbit cornea assay [11]. In experimental breast cancer bone metastases, cilengitide was shown to reduce the size of osteolytic lesions and the corresponding soft tissue tumors [12].

Metabolic imaging with positron emission tomography (PET) is an established method in addition to anatomic imaging methods in patients with several tumor types, including metastatic breast cancer. Several studies have been performed to assess the impact of transporters and hexokinases on the glucose or fluorine-18 fluorodeoxyglucose ($^{18}$F-FDG) kinetics, which suggested a modulation of the FDG kinetics by angiogenesis-related genes [13]. Moreover, prior studies from other groups have suggested that serial measurements of tumor glucose metabolism using $^{18}$F-FDG PET are helpful for monitoring breast cancer tumor response [14-18]. MicroPET imaging of breast cancer αv integrin expression with $^{64}$Cu-labeled dimeric Arg-Gly-Asp (RGD) peptides has been reported also [19].

The rationale of this experimental study was the assessment of the $^{18}$F-FDG kinetics based on quantitative PET for the evaluation of treatment effects of an integrin antagonist in the setting of experimental metastatic breast cancer. Previously, we have studied early effects of FOLFOX treatment of colorectal tumor in an animal model by assessment of $^{18}$F-FDG kinetics [20]. The present study was undertaken to monitor therapeutic effects in individual rats with breast cancer bone metastases after cilengitide treatment and to detect combinations of PET parameters that may be helpful in identifying the treatment effect by PET follow-up studies with $^{18}$F-FDG. The uptake of $^{18}$F-FDG is a sensitive indicator of alterations in glucose metabolism in tumors. However, whether PET with $^{18}$F-FDG may be able to assess the effects of cilengitide treatment is still unresolved. Furthermore, the impact of a short-term cilengitide treatment on the individual parameters of $^{18}$F-FDG kinetics is not known. Therefore, the animal experiments were designed to assess effects of cilengitide treatment on $^{18}$F-FDG kinetics.

## Materials and methods

### Animal characteristics, treatment

Experiments were approved by the responsible governmental animal ethics committee. Nude rats were obtained from Harlan Winkelmann GmbH (Borchen, Germany) at an age of 6 weeks. The human estrogen-independent breast cancer cell line MDA-MB-231 was obtained from the American Type Culture Collection. The experimental model to induce breast cancer bone metastases was performed as described before [21]. Briefly, nude rats were inoculated with $10^5$ MDA-MB-231 breast cancer cells into the superficial epigastric artery. Osteolytic metastases in the respective hind leg occurred within 30 days after the cancer cell inoculation. Dynamic PET studies with $^{18}$F-FDG were performed in all animals after tumor cell inoculation. The whole study comprised of 9 untreated (day 30 after tumor cell inoculation), 4 controlled (sham-treated, day 55 after tumor cell inoculation) and 6 treated (day 55 after tumor cell inoculation) rats. The integrins αvβ3 and αvβ5 inhibitor cilengitide (Merck, Darmstadt, Germany) was applied intraperitoneally (75 mg/kg body weight, five times per week) from day 30 to 55 after tumor cell inoculation. Tumor-bearing controlled animals received saline injections instead of cilengitide. During processing, rats were anesthetized using a mixture of nitrous oxide (1 l/min), oxygen (0.5 l/min) and isoflurane (1.5 vol%).

### Magnetic resonance imaging

T2-weighted imaging was performed using a turbo spin echo sequence (orientation axial, TR 3240ms, TE 81ms, matrix 152x256, FOV 90x53.4mm2, slice thickness 1.5mm, 3 averages, scan time 3min 40sec). The volumes of soft tissue components, expressed in mL, were determined from MRI-acquired T2-weighted images using Medical Imaging Interaction Toolkit (MITK, Heidelberg, Germany).

### PET, kinetic model

The PET acquisition parameters have been described elsewhere [13, 20] and are summarized briefly here. The standard $^{18}$F-FDG-PET protocol at our institute is based on dynamic data acquisition for 60min beginning from the intravenous injection of 1.80-5.67MBq $^{18}$F-FDG and is a 28-frame protocol (ten frames of 30sec, five frames of 60sec, five frames of 120sec and eight frames of 300sec). A dedicated PET system (ECAT EXACT HR+; Siemens, Erlangen, Germany) with an axial field of view of 15.3cm operated in 2D mode was used for all animal studies. The system provides the simultaneous acquisition of 63 transverse slices with a slice thickness of 2.4mm. The animals were positioned in the axial plane of the system to maintain the best resolution in the center of the system. A transmission scan (10min) was obtained prior to radionuclide administration for attenuation correction of the acquired dynamic emission data. The software developed at our center was used to reconstruct images iteratively using the ordered-subset expectation maximization algorithm (6 iterations, 2 subsets), and the median root prior correction was applied to the intermediate matrices, which limits the dependency of the pixel maximum from the number of iteration steps. The theoretic voxel size was 2.277x2.277x2.425mm. The reconstructed images were converted to standardized uptake value (SUV) images based on the formula [22]: *SUV = Tissue concentration (Bq/g)/[injected dose (Bq)/body weight (g)]*. The SUV images were used for all further quantitative evaluations. Learning machine two-tissue compartmental modeling was performed with dynamic PET data. The SUV 55-60min following $^{18}$F-FDG injection was used for the assessment of $^{18}$F-FDG uptake.

In animals, a partial volume correction must be applied to the data due to the small size of the input and tumour volumes of interest (VOI). Herein, the recovery coefficient was 0.85 for a diameter of 8mm and 0.32 for a diameter of 3mm based on phantom measurements as well as the recent parameter settings used with our reconstruction software. A partial volume correction function was previously calculated for our PET system using phantom measurements and was used to correct the dynamic data obtained in this study. For the input function the mean values of the VOI data obtained from the heart were used. We used a preprocessing tool which allowed a fit of the input curve by a sum of up to three decaying exponentials. The learning-machine two-tissue compartment model provides five parameters: the transport parameters for $^{18}$F-FDG into and out of the cell, K1 and k2, the parameters for phosphorylation and dephosphorylation of intracellular $^{18}$F-FDG, k3 and k4, and the fractional blood volume, also called vessel density (VB), which reflects the amount of blood in the VOI. Following compartment analysis, we calculated the global influx of $^{18}$F-FDG from the compartment data using the formula: *influx = (K1*k3)/(k2+k3).* A machine learning method was used for the fitting, which has the advantage of a fast convergence and avoidance of over fitting as compared to the standard iterative method [23].

### Statistical analysis

Statistical evaluation was performed with Stata/SE 10.1 (stataCorp, College Station, TX) using the descriptive statistics and scatter plots. The classification analysis was performed using the GenePET software [24]. The software applies the support vector machines (SVM) algorithm and provides a classification analysis by optimising a hyperplane between the target variables. The algorithm for selection or elimination of variables, the feature ranking, can be based on different criteria, e.g. F-test, Mann-Whitney test, or the SVM ranking feature elimination (SVM_RFE) approach [25]. The SVM_RFE algo-

rithm computes a multidimensional weight vector for the PET variables and the square of the vector is used to calculate the ranking criteria. The overall accuracy, which reflects the correctness of the classification of untreated, controlled and treated animals in relation to the total number of samples, was used to assess the results of the SVM analysis. For comparison between two groups, the two-sided Wilcoxon rank sum test was applied for all kinetic PET parameters, SUV and tumor size, using a single parameter analysis. P values <0.05 were considered significant.

## Results

### Single parameter analysis

The mean, median, minimum and maximum values as well as the standard deviation of quantitative PET parameters for the $^{18}$F-FDG kinetics in controlled and treated animals were presented in Table 1. All data considering untreated animals are presented in the supporting material. Herein, owing to the death of untreated rats, the sample size of the controlled group was smaller than that of untreated and treated animals. Obviously, the SUV was decreased in treated animals as compared with the controlled group. In addition, a box plot of kinetic data (Fig. 1) showed the value of VB and K1 in treated animals was higher than that of controlled animals, but the value of k3 and INF was lower.

Using $P<0.05$ as the significance level, the Wilcoxon rank-sum test revealed that statistically significant differences were found for the transport rate K1 and the phosphorylation rate k3 between controlled and treated animals ($P=0.033$ and 0.038; Table 2). In addition, a statistically significant difference was found for the tumor volume from MRI as demonstrated on Table 2 ($P=0.011$).

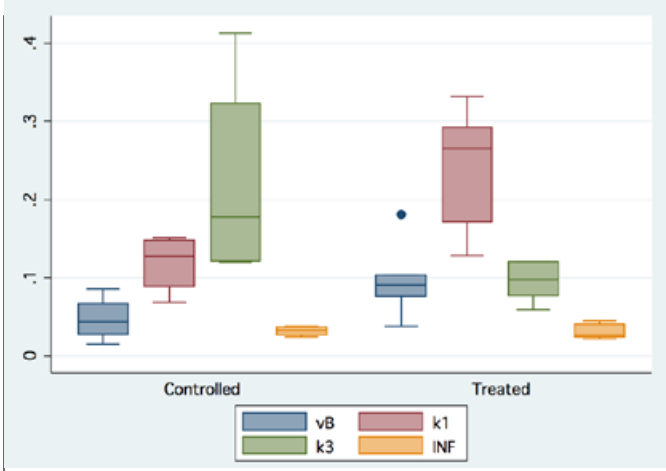


**Figure 1.** Box plot of kinetic data in controlled and treated animals. The value of VB and K1 in treated animals was higher than that of controlled animals, but the value of k3 and INF was lower.

### Multiparameter analysis

Besides the single parameter analysis, a multiparameter analysis was performed to assess the possible impact of treatment on $^{18}$F-FDG kinetic data. The SVM algorithm was used for classification analysis with the Mann-Whitney test as the feature ranking procedure and the Mann-Whitney test for the kernel function. The aim was to identify a combination of variables that would discriminate controlled and treated animals.

The highest overall accuracy of 80.0% was achieved for a combination of k2 and VB between treated and controlled rats. Of the 6 treated animals, 5 were correctly identified and of the 4 controlled animals, 3 were correctly identified based on the combination of k2 and VB. All results are shown in Table 3.

**Table 1.** Quantitative PET parameters for the $^{18}$F-FDG kinetics in controlled (n=4) and treated animals (n=6)

| Group | | VB | K1 | K2 | K3 | K4 | Influx | SUV | Tumor volume (mL) | No. |
|---|---|---|---|---|---|---|---|---|---|---|
| Controlled | Mean | 0.047 | 0.119 | 0.462 | 0.222 | 0.013 | 0.032 | 2.573 | 4.065 | 4 |
| | SD | 0.029 | 0.038 | 0.076 | 0.137 | 0.008 | 0.006 | 0.550 | 2.687 | 4 |
| | Median | 0.044 | 0.127 | 0.373 | 0.178 | 0.010 | 0.033 | 2.632 | 2.632 | 4 |
| | Minimum | 0.015 | 0.069 | 0.555 | 0.120 | 0.008 | 0.025 | 1.902 | 2.521 | 6 |
| | Maximum | 0.085 | 0.151 | 0.626 | 0.413 | 0.024 | 0.038 | 3.127 | 7.575 | 6 |
| Treated | Mean | 0.097 | 0.243 | 0.626 | 0.096 | 0.015 | 0.031 | 2.119 | 0.310 | 6 |
| | SD | 0.047 | 0.078 | 0.121 | 0.025 | 0.006 | 0.010 | 0.392 | 0.267 | 6 |
| | Median | 0.091 | 0.266 | 0.634 | 0.098 | 0.015 | 0.027 | 2.098 | 0.211 | 6 |
| | Minimum | 0.038 | 0.128 | 0.461 | 0.060 | 0.006 | 0.022 | 1.687 | 0.053 | 6 |
| | Minimum | 0.181 | 0.332 | 0.760 | 0.121 | 0.023 | 0.045 | 2.573 | 0.670 | 6 |

**Table 2.** The value of statistically significant level P using the Wilcoxon rank-sum test. P values <0.05 were considered significant*

| P | | | | | | | |
|---|---|---|---|---|---|---|---|
| VB | K1 | K2 | K3 | K4 | Influx | SUV | Tumor volume |
| 0.088 | 0.033* | 0.055 | 0.038* | 0.670 | 0.670 | 0.201 | 0.011* |

**Table 3.** The classification results based on SVM_RFE with highest accuracy. PPV: positive predictive value, NPV: negative predictive value

| Parameters | Sensitivity | Specificity | PPV | NPV | Accuracy |
|---|---|---|---|---|---|
| VB, k2 | 3/4 (75.0%) | 5/6 (83.3%) | 3/4 (75.0%) | 5/6 (83.3%) | 8/10 (80.0%) |

Representative SUV images of $^{18}$F-FDG uptake from three groups' animals (Fig. 2a) revealed a larger bone metastasis in the hind leg of a controlled animal as compared to an untreated rat. Furthermore, the functional volume of the skeletal metastasis in a treated animal **was** slightly larger than that in the untreated but clearly smaller than in the controlled animal, which is consistent with data in Table 1 and the MRI images (Fig. 2b).

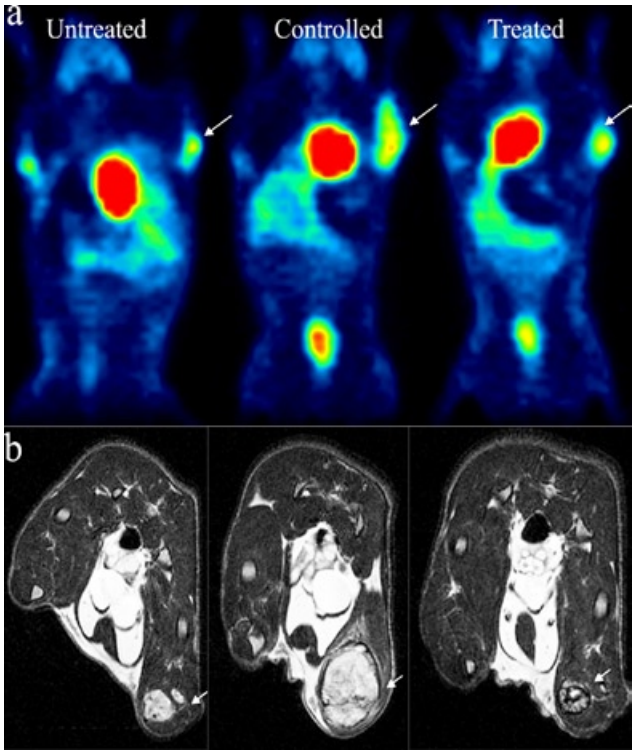


**Figure 2.** Representative SUV images of $^{18}$F-FDG uptake (**a**) and MRI T2-weighted images (**b**) in axial orientation from three groups' animals (see the right leg, arrows point at bone metastases).

## Discussion

Positron emission tomography with $^{18}$F-FDG is recommended for the primary diagnosis, staging, evaluation of relapse and assessment of treatment response in patients with different tumors including breast cancer, colorectal cancer or soft-tissue sarcomas [26-28]. Cilengitide is a cyclic peptide containing the sequence RGDf(N-Me)V with high affinity for αvβ3 and αvβ5 integrins, which are important in angiogenesis and metastasis [29]. In experimental breast cancer bone metastases, cilengitide inhibited the growth of skeletal lesions as shown by CT and MRI [12]. The aim of this study was to examine the value of a dynamic, quantitative $^{18}$F-FDG study using several pharmacokinetic parameters for assessment of the treatment effect of cilengitide in experimental breast cancer bone metastases.

Quantitative PET provides the possibility to assess pharmacokinetic data. A two-tissue-compartment model is a generally accepted method for an accurate, detailed kinetic analysis of the $^{18}$F-FDG metabolism. The $^{18}$F-FDG, as a glucose analog, is taken up by high-glucose-using cells such as brain, kidney, and cancer cells, where phosphorylation prevents the glucose from being released again from the cell, once it has been absorbed [30]. The size of a tumor as well as the system resolution should influence all parameters. Herein, we implemented a new method for the two-tissue-compartment fitting of VOI, which is based on a machine learning method [23]. Thus the critical selection of the starting values could be solved by an observer-independent method, which guarantees that the interobserver and intraobserver error is generally low compared with an iterative solution method. Furthermore, a partial volume correction was applied to the data due to the small size of the input and tumor VOI, which guarantees the accurate measurement of the input and tumor functions.

Schwarzbach et al. (2000) reported that the SUV was helpful in the diagnosis of primary and recurrent high-grade tumors [31]. In our study, a decrease in SUV, referring to metabolic downregulation was found in cilengitide-treated rats when compared to controlled animals. This result indicated an effect of cilengitide treatment on the global $^{18}$F-FDG-metabolism. However, the SUV values did not differ significantly between the controlled and treated groups. As we know, one limitation of the SUV is the differentiation of low-grade sarcomas or at least a subset of low-grade soft-tissue tumors because sarcomas are a histologically heterogeneous group. Depending on the histology, $^{18}$F-FDG uptake and phosphorylation may be different for the various histological subtypes. Thus, in this study, several kinetic parameters obtained from the dynamic $^{18}$F-FDG data provided more insight into the mechanism of action of cilengitide. The transport constants K1 and k2 are primarily parameters for the transport capacity of $^{18}$F-FDG, and the rate constant k3 is associated with the phosphorylation rate of the radiopharmaceutical. The blood volume in tumors is a parameter that modulates the uptake of the tracer. Therefore, the use of the vascular fraction (VB) of a target volume is another parameter that may improve diagnostic accuracy. In our study, we showed that the value of VB and K1 in treated animals was higher than that of controlled animals, but the value of k3 and INF was lower, which indicated successful treatment. Moreover, K1 and k3 showed significant differences between treated and controlled rats. Torizuka et al. (1998) suggested that k3 is the rate-limiting factor in $^{18}$F-FDG accumulation in untreated breast cancers rather than other PET parameters [32]. In our series, however, we found that K1 was most sensitive for therapeutic changes among all parameters as far as the significance levels were concerned. Thus, there was a shift in the $^{18}$F-FDG kinetic pattern after treatment, driven by glucose delivery (K1) relative to the rate of phosphorylation (k3). It is safe to say that the cilengitide treatment reduced glucose metabolism and slowed tumor growth in accordance with previous results [12].

Moveover, after treatment using cilengitide in our experimental model, mean k3 ($P<0.05$) and INF ($P>0.05$) declined, whereas mean K1 ($P<0.05$) increased. An increase in K1 was in discordance with our previous results in colorectal cancer, which demonstrated that K1 is related to angiogenesis [13]. A possible explanation was that cilengitide might have a higher impact on proliferation or cell migration than on angiogenesis. In addition, the observed effect of cilengitide might be the inhibition of interactions between αv integrins and the respective binding partners such as bone sialoprotein (BSP) and matrix metalloproteinases (MMP) [33]. The integrins αvβ3 and αvβ5 are interaction partners of BSP, which is considered to play an important role in the pathogenesis of breast, prostate or lung cancer patients concerning tumor cell adhesion, progression and invasion [33-37]. Furthermore αvβ3 was observed to form complexes with MMP-2, which increased the invasive potential of breast cancer cells [38]. A decrease in viability of MDA-MB-231 breast cancer cells after treatment with cilengitide as observed in our study might therefore be owed to the αvβ3 and αvβ5 inhibition including the blocking of its binding partners. The exact mechanism of action of cilengitide in our model, however, remains to be elucidated.

We demonstrated that tumor volume as assessed by MRI was a sensitive parameter for differentiating treated and controlled animals. However, changes in tumor volume do not provide any data of the biological mechanisms, which are responsible for any therapeutic effects. Dynamic $^{18}$F-FDG-PET parameters provide information about early metabolic changes of a therapeutic drug [20, 28]. Furthermore, differences in the skeletal lesion size of bone metastases appear rather late after therapeutic intervention [39]. Therefore, novel imaging biomarkers are needed for assessment of treatment response, which are independent of morphology.

Our results indicated that PET might be of clinical value for the assessment of treatment response to cilengitide in patients with breast carcinoma metastases. Further studies will elucidate, if effects upon cilengitide treatment can be captured earlier using PET than by assessment of morphology alone.

It was concluded that compartment analysis of $^{18}$F-FDG-PET studies in a tumor model was helpful to assess changes induced by a targeted treatment against αv integrins. PET parameters provided a new tool for gaining insight in the mechanism of action of cilengitide in bone metastases and might be used for assessment of treatment response in skeletal and visceral metastases. Furthermore, the analysis of $^{18}$F-FDG-PET parameters could be helpful for assessment and management of cilengitide treatment in patients with metastatic breast cancer. Further studies will explore biologic mechanisms underlying our findings using techniques such as *in vitro* assays, immunohistochemical analysis as well as non-invasive imaging methods, which should be highly suitable for monitoring all aspects of bone metastases.

Supporting Material: *Quantitative PET parameters for the $^{18}$F-FDG kinetics in untreated animals (n=9)*

*Acknowledgements*
We thank Karin Leotta, Renate Bangert and Lisa Seyler for excellent technical assistance. We furthermore thank the Deutsche Forschungsgemeinschaft (SFB-TR23) and Merck-Serono for financial support.

*All authors declare that they have no conflicts of interest*

## Bibliography

1. Jemal A, Siegel R, Ward E et al. Cancer statistics 2006. *CA Cancer J Clin* 2006; 56: 106-30.
2. Wedam SB, Low JA, Yang SX et al. Antiangiogenic and antitumor effects of bevacizumab in patients with inflammatory and locally advanced breast cancer. *J Clin Oncol* 2006; 24: 769-77.
3. Bäuerle T, Hilbig H, Bartling S et al. Bevacizumab inhibits breast cancer-induced osteolysis, surrounding soft tissue metastasis, and angiogenesis in rats as visualized by VCT and MRI. *Neoplasia* 2008; 10: 511-20.
4. Piccart-Gebhart MJ, Procter M, Leyland-Jones B et al. Trastuzumab after adjuvant chemotherapy in HER2-positive breast cancer. *N Engl J Med* 2005; 353: 1659-72.
5. Geyer CE, Forster J, Lindquist D et al. Lapatinib plus capecitabine for HER2-positive advanced breast cancer. *N Engl J Med* 2006; 355: 2733-43.
6. Baselga J, Swain SM. Novel anticancer targets: Revisiting ERBB2 and discovering ERBB3. *Nat Rev Cancer* 2009; 9: 463-75.
7. Chambers AF, Groom AC, Macdonald IC. Metastasis: Dissemination and growth of cancer cells in metastatic sites. *Nat Rev Cancer* 2002; 2: 563-72.
8. Avramides CJ, Garmy-Susini B, Varner JA. Integrins in angiogenesis and lymphangiogenesis. *Nat Rev Cancer* 2008; 8: 604-17.
9. Pecheur I, Peyruchaud O, Serre CM et al. Integrin alpha(v)beta3 expression confers on tumor cells a greater propensity to metastasize to bone. *Faseb J* 2002; 16: 1266-8.
10. Sloan EK, Pouliot N, Stanley KL et al. Tumor-specific expression of alphavbeta3 integrin promotes spontaneous metastasis of breast caner to bone. *Breast Cancer Res* 2006; 8: R20.
11. Germer M, Kanse SM, Kirkgaard T et al. Kinetic analysis of integrin-dependent cell adhesion on vitronectin: The inhibitory

**Supporting Material:** Quantitative PET parameters for the $^{18}$F-FDG kinetics in untreated animals (n=9)

| Group | | VB | K1 | K2 | K3 | K4 | Influx | SUV | Tumor size (mL) | No. |
|---|---|---|---|---|---|---|---|---|---|---|
| Untreated | Mean | 0.095 | 0.253 | 0.574 | 0.079 | 0.016 | 0.028 | 2.552 | 0.349 | 9 |
| | SD | 0.048 | 0.092 | 0.160 | 0.050 | 0.011 | 0.012 | 0.703 | 0.340 | 9 |
| | Median | 0.098 | 0.281 | 0.614 | 0.072 | 0.014 | 0.028 | 2.457 | 0.228 | 9 |
| | Minimum | 0.042 | 0.063 | 0.190 | 0.016 | 0.005 | 0.005 | 1.732 | 0.008 | 9 |
| | Minimum | 0.200 | 0.359 | 0.734 | 0.198 | 0.039 | 0.051 | 3.533 | 1.093 | 9 |

potential of plasminogen activator inhibitor-1 and RGD peptides. *Eur J Biochem* 1998; 253: 669-74.
12. Bäuerle T, Komljenovic D, Merz M et al. Cilengitide inhibits progression of experimental breast cancer bone metastases as imaged non-invasively using VCT, MRI and DCE-MRI in a longitudinal *in vivo* study. *Int J Cancer* 2010; Doi: 10.1002/ijc. 25563.
13. Strauss LG, Koczan D, Klippel S et al. Impact of angiogenesis-related gene expression on the tracer kinetics of $^{18}$F-FDG in colorectal tumors. *J Nucl Med* 2008; 49: 1238-44.
14. Wahl R, Zasadny K, Helvie M et al. Metabolic monitoring of breast cancer chemohormonotherapy using positron emission tomography: initial evaluation. *J Clin Oncol* 1993; 11: 2101-11.
15. Bassa P, Kim E, Inoue T et al. Evaluation of preoperative chemotherapy using PET with fluorine-18-fluorodeoxyglucose in breast cancer. *J Nucl Med* 1996; 37: 931-8.
16. Jansson T, Westlin JE, Ahlstrom H et al. Positron emission tomography studies in patients with locally advanced and/or metastatic breast cancer: a method for early therapy evaluation? *J Clin Oncol* 1995; 13: 1470-7.
17. Smith IC, Welch AE, Hutcheon AW et al. Positron emission tomography using $^{18}$F-fluorodeoxy-D-glucose to predict the pathologic response of breast cancer to primary chemotherapy. *J Clin Oncol* 2000; 18:1676-88.
18. Schelling M, Avril N, Nahrig J et al. Positron emission tomography using $^{18}$F fluorodeoxyglucose for monitoring primary chemotherapy in breast cancer. *J Clin Oncol* 2000; 18: 1689-95.
19. Chen X, Liu S, Hou Y et al. MicroPET imaging of breast cancer alphav-integrin expression with $^{64}$Cu-labeled dimeric RGD peptides. *Mol Imaging Biol* 2004; 6: 350-9.
20. Strauss LG, Hoffend J, Koczan D et al. Early effects of FOLFOX treatment of colorectal tumor in an animal model: assessment of changes in gene expression and FDG kinetics. *Eur J Nucl Med Mol Imaging* 2009; 36: 1226-34.
21. Bäuerle T, Adwan H, Kiessling F et al. Characterization of a rat model with site-specific bone metastasis induced by MDA-MB-231 breast cancer cells and its application to the effects of an antibody against bone sialoprotein. *Int J Cancer* 2005; 115: 177-86.
22. Strauss LG, Conti PS. The applications of PET in clinical oncology. *J Nucl Med* 1991; 32: 623-48.
23. Pan L, Mikolajczyk K, Strauss LG et al. Machine learning based parameter imaging and kinetic modelling of PET data. *J Nucl Med* 2007; 48 (suppl 2): 158P.
24. Strauss LG, Pan L, Koczan D et al. Fusion of positron emission tomography (PET) and gene array data: a new approach for the correlative analysis of molecular biological and clinical data. *IEEE Trans Med Imaging* 2007; 26: 804-12.
25. Guyon I, Weston J, Barnhill S et al. Gene selection for cancer classification using support vector machines. *Mach Learn* 2002; 46: 389-422.
26. Kasper B, Hohenberger P, Strauss LG, Dimitrakopoulou-Strauss A. The use of fluorine-18 fluorodesoxyglycose-positron emission tomography for treatment monitoring in patients with soft tissue sarcomas. *Hell J Nucl Med* 2010; 37: 1876-82.
27. Dimitrakopoulou-Strauss A, Pan L, Strauss LG. Parametric imaging: a promising approach for the evaluation of dynamic PET-18F-FDG studies - the DKFZ experience. *Hell J Nucl Med* 2010; 13: 18-22.
28. Dimitrakopoulou-Strauss A, Strauss L. Quantitative studies using positron emission tomography (PET) for the diagnosis and therapy planning of oncological patients. *Hell J Nucl Med* 2006; 9: 10-21.
29. Xiong JP, Stehle T, Zhang R et al. Crystal Structure of the Extracellular Segment of Integrin V3 in Complex with an Arg-Gly-Asp Ligand. *Science* 2002; 296: 151-5.
30. Hawkins RA, Choi Y, Hung S et al. Quantitating Tumor Glucose Metabolism with FDG and PET. *J Nucl Med* 1992; 33: 339-44.
31. Schwarzbach M, Dimitrakopoulou-Strauss A, Willeke F et al. Clinical value of $^{18}$F-fluorodeoxyglucose positron emission tomography imaging in soft tissue sarcomas. *Ann Surg* 2000; 231: 380-6.
32. Torizuka T, Zasadny KR, Recker B et al. Untreated primary lung and breast cancers: correlation between $^{18}$F- FDG kinetic rate constants and findings of in vitro studies. *Radiology* 1998; 207: 767-74.
33. Karadag A, Ogbureke KU, Fedarko NS et al. Bone sialoprotein, matrix metalloproteinase 2, and alpha(v)beta3 integrin in osteotropic cancer cell invasion. *J Natl Cancer Inst* 2004; 96: 956-65.
34. Egeblad M, Werb Z. New functions for the matrix metalloproteinases in cancer progression. *Nat Rev Cancer* 2000; 2: 161-74.
35. Tester AM, Waltham M, Oh SJ et al. Pro-matrix metalloproteinase-2 transfection increases orthotopic primary growth and experimental metastasis of MDA-MB-231 human breast cancer cells in nude mice. *Cancer Res* 2004; 64: 652-8.
36. Hood JD, Cheresh DA. Role of integrins in cell invasion and migration. *Nat Rev Cancer* 2002; 2: 91-100.
37. Pecheur I, Peyruchaud O, Serre CM et al. Integrin alpha(v)beta3 expression confers on tumor cells a greater propensity to metastasize to bone. *FASEB J* 2002; 16: 1266-8.
38. Brooks PC, Stromblad S, Sanders LC et al. Localization of matrix metalloproteinase MMP-2 to the surface of invasive cells by interaction with integrin alpha v beta 3. *Cell* 1996; 85: 683-93.
39. Bäuerle T, Semmler W. Imaging response to systemic therapy for bone metastases. *Eur Radiol* 2009; 19: 2495-507.